Article:
Yao, S, Xu, Y orcid.org/0000-0001-5180-8892, Zhou, Y et al. (7 more authors) (2019) Calcium Phosphate Nanocluster-Loaded Injectable Hydrogel for Bone Regeneration. ACS Applied Bio Materials, 2 (10). pp. 4408-4417. ISSN 2576-6422

https://doi.org/10.1021/acsabm.9b00270

Calcium phosphate nanocluster-loaded injectable hydrogel for bone regeneration

Shasha Yao,[†] Yifei Xu,[‡,§] Yanyan Zhou,[&] Changyu Shao,[†] Zhaoming Liu,[†] Biao Jin,[†] Ruibo Zhao,[†] Han Cao,[†] Haihua Pan,[†] and Ruikang Tang[*,†]

[†] Center for Biomaterials and Biopathways, Department of Chemistry, Zhejiang University, Hangzhou, Zhejiang 310027, China

E-mail: rtang@zju.edu.cn

[‡] Laboratory of Materials and Interface Chemistry and Center for Multiscale Electron Microscopy, Department of Chemical Engineering and Chemistry, Eindhoven University of Technology, Eindhoven, PO box 513, 5600 MB Eindhoven, The Netherlands

[§] Institute for Complex Molecular Systems, Eindhoven University of Technology, Eindhoven, PO box 513, 5600 MB Eindhoven, The Netherlands

[&] Department of Oral Medicine, Affiliated Hospital Stomatology, School of Medicine, Zhejiang University, Hangzhou, Zhejiang 310012, China.

KEYWORDS: calcium phosphate, nanocluster, injectable, hydrogel, bone regeneration

ABSTRACT

Bone is a hierarchical tissue in which the extracellular matrix consists of hydroxyapatite (HAP) crystals embedded in the collagen matrix. Artificial bone regeneration remains a great challenge due to the difficulty of balancing the chemical composition, biological compatibility and mechanical performance of the implant. Biomineralization starts from the formation of a hydrogel-like bio-macromolecule matrix in many cases, while the mineralization of HAP often builds from amorphous calcium phosphate (ACP) nanoclusters. Inspired by these discoveries, here we use a hydrogel loaded with ~1 nm sized polymer-stabilized ACP nanoclusters (cluster-loaded hydrogel) as an injectable bone regeneration material. The hydrogel is biocompatible and stabilizes the ACP clusters such that they could efficiently infiltrate into collagen fibrils leading to intrafibrillar mineralization of HAP nanocrystals. The ex vivo results reveal that the cluster-loaded hydrogel has an excellent bone affinity as well as provide a suitable environment for the proliferation and differentiation of bone cells. In vivo experiments with rat bone show that the cluster-loaded hydrogel can generate HAP-based fillings within bone defects with perfect bonding to the surrounding tissue and a mechanical performance comparable with native bone. The fluidity of the hydrogel is further beneficial by providing a feasible minimally invasive bone healing procedure via syringe injection. The discovery and utilization of the cluster-loaded hydrogel described here provides a promising bio-inspired approach for bone tissue regeneration.

1. INTRODUCTION

Bone is a hierarchical tissue whose extracellular matrix consists of type-I collagen fibrils embedded with oriented hydroxyapatite (HAP) crystals.[1,2] Damage to this biological tissue leads

to dysfunction associated with significant economic costs.[3] Since bone itself has limited innate ability to mount a healing response, bone reconstruction is an important research target.[4] Although current biomedical bone regeneration relies largely on the integration of allogeneic grafts and synthetic substitutes composed of metallic,[5] ceramic,[6] and polymeric scaffold materials,[7,8] in the past few decades, hydrogels have emerged as promising scaffold precursors for bone regeneration due to their inherent flexibility and biocompatibility.[9-11]

In bone as well as several other biomineralization systems,[12-16] the hydrogel nature of the extracellular matrix is thought to play a significant role in regulating the mineralization process by modulating diffusion rates, ion activities, and water structure,[17] making synthetic calcium phosphate loaded hydrogel a promising platform for bone regeneration.[18-22] It however remains a great challenge to connect hydrogel-based bone repair materials perfectly to the boundaries of bone defects and effectively remineralize the damaged matrix in order to generate continuous HAP fillings with satisfactory mechanical properties comparable to native bone.

Based on cryo-transmission electron microscopy (cryoTEM) studies, collagen mineralization has been proposed to start from the formation of ~1 nm sized amorphous calcium phosphate (ACP) nanoclusters.[23-25] Other ex vivo studies have shown that with the presence of charged polymers such as poly(allylamine hydrochloride) (PAH),[26] polyacrylic acid (PAA),[27] or polyaspartic acid (PASP),[23,28] ACP clusters can be stabilized and facilitate the formation of oriented intrafibrillar HAP nanoplatelets.[29,30] Inspired by these findings, we suggest that a hydrogel of charged polymers loaded with a high concentration of ACP nanoclusters could be used as a precursor for bone regeneration via a biomineralization-like pathway.

2. EXPERIMENTAL SECTION

2.1. Synthesis of ACP nanocluster-loaded injectable hydrogel (cluster-loaded hydrogel). Calcium chloride ($CaCl_2$), disodium hydrogen phosphate (Na_2HPO_4), sodium hydroxide (NaOH) and PAA (Mw = 450 000 Da) were purchased from Sigma-Aldrich (Beijing, China). PASP (Mw = 9 000–11 000 Da) was from Ai-ke Chemicals (Chengdu, China).

To prepare the cluster-loaded hydrogel, a mixed solution of 2 mL 0.1 M Na_2HPO_4, 0.4 mL 0.3 g/mL PAA and 0.15 g/mL PASP were slowly injected into a vigorously stirring solution of 0.1 M $CaCl_2$ and 0.2 mL 0.3 g/mL PASP under ambient conditions, and then the pH value was adjusted to 7.4 with a 3 M NaOH solution.

2.2. Rheological analysis. Rheological measurement of the cluster-loaded hydrogel was carried out by using an Anton Paar rheometer (DHR, TA, USA). The samples were placed between parallel plates of 15 mm diameter with a gap of 1 mm. The storage modulus (G') and loss modulus (G'') were measured to test the rheological properties.

2.3. Collagen mineralization. To assemble collagen fibrils on 300-mesh nickel TEM grids, 8.33 μL of collagen stock solution was mixed with 0.5 mL of assembling buffer solution and incubated for 20 min. Then, 3 μL of incubated collagen solution was dripped onto the 300-mesh nickel TEM grids and incubated at 37 ^{o}C for 16 h. The collagen-coated TEM grids were further cross-linked with 0.05% glutaraldehyde for 4 h and rinsed with deionized water. After that, the collagen-coated TEM grids were floated on the cluster-loaded hydrogel for mineralization at 37 ^{o}C for different times. Then, the collagen-coated TEM grids were washed with deionized water, dried at room temperature and kept for further experiments.

2.4. Cell culture. Mouse calvarial-derived preosteoblastic cells (MC3T3-E1; ATCC CRL-2593) were cultured in alpha minimum essential medium (α-MEM) supplemented with 10% foetal

bovine serum (FBS) and 1% penicillin/strepto-mycin. Three types of media were prepared for the culture: disperse 5 mg cluster-loaded hydrogel into 50 mL α-MEM medium to obtain a 100 μg/mL of cluster-loaded hydrogel dispersion (cluster-loaded hydrogel group); suspend 5 mg of HAP particles in 50 mL of α-MEM medium to get 100 μg/mL of HAP suspension (HAP group); and α-MEM medium only (control group). The medium was changed every other day, and the cultures were incubated at 37 ^{o}C in a humidified atmosphere containing 5% CO_2. All cell-culture-related reagents were purchased from Gibco. A haemocytometer was used to determine the cell density before each experiment.

2.5. Cell viability assay. MC3T3-E1 cells with cluster-loaded hydrogel were incubated in 96-well plates, and MC3T3-E1 cells in the suspension of HAP medium and medium only were used as the control groups. Approximately 5 000 cells were seeded in each well and cultured in 150 μL of the three above-mentioned different media for different times. The cell viability was measured by cell counting kit-8 (CCK-8). After 1, 3, 5, and 7 days of incubation, the medium was removed and 90 μL of fresh medium and 10 μL of CCK-8 were added to each well and incubated at 37 ^{o}C and 5% CO_2 for 2 h. Then, 100 μL of culture media was removed from each well and transferred to another 96-well plate. The absorbance of the samples was measured at 490 nm by a spectrophotometric microplate reader (Bio-Rad 680, USA).

2.6. Live/dead assay. A total of 10 000 MC3T3-E1 cells were seeded in 24 well plates and cultured with cluster-loaded hydrogel medium, suspension of HAP medium, or medium only at 37 ^{o}C in a humidified atmosphere of 5% CO_2 and grown for 1, 3, 5, and 7 days. The staining solution was prepared for live/dead staining. MC3T3-E1 cells without materials were used as positive controls, and negative control of MC3T3-E1 cells were treated with 70% of methanol for 30 min. The culture medium was removed, and cells were washed three times with 500 μL of phosphate-

buffered saline (PBS). Then, 400 μL of the staining solution was added to each well and incubated for 40 min while protected from light. A Zeiss Axio Imager M2 (Carl Zeiss Microscopy GmbH, Goettingen, Germany) was used to take photographs of the live/dead assay. All cell experiments were performed in triplicate.[31]

2.7. Pro-inflammatory cytokines (IL-6). IL-6 is a pleiotropic cytokine produced in response to inflammatory stimuli and is mostly excreted from immune cells such as helper T cells (Th) and macrophages, and other cell types that promote inflammation.[32] In order to test the inflammatory response, RAW264.7 cells were cultured with the cluster-loaded hydrogel, HAP suspension, and control groups at 37 ^{o}C for 1, 6, and 24 h, respectively. Then, we recovered the supernatants and assessing the concentration of IL-6 by using a Mouse IL-6 ELISA Kit (4A Biotech, Beijing) according to the manufacturer's instructions.

2.8. Quantitative real time qPCR analysis. MC3T3-E1 cells were seeded in 12 well plates and cultured with the cluster-loaded hydrogel, HAP suspension, and control groups. To induce osteogenic differentiation, the medium was supplemented with 50 μM ascorbic acid (Sigma-Aldrich), 10 mM β-glycerol phosphate (Sigma-Aldrich), and 0.1 μM dexamethasone (Sigma-Aldrich). When the cells were grown for 3, 7, and 14 days, the RNA was extracted using TRIzol Ambion (Invitrogen, USA) and quantified using a spectrophotometer (NanoDrop2000; Thermo Scientific, Waltham, MA, USA). Subsequently, cDNA was synthesized using an iScript cDNA Synthesis Kit (Bio-Rad, USA). Finally, qPCR was performed using the Bio-Rad CFX384 PCR System (Bio-Rad, USA) and the expression level of the osteogenic markers was quantified with iTaq^{TM} Universal SYBR Green SuperMix (Bio-Rad, USA). The sequences of the specific primers used are shown in Table 1. The expression values were normalized to GAPDH (B66130, Sangon, Shanghai).

Table 1

qPCR genes and primer sequences used for MC3T3-E1 mouse preosteoblasts.

Gene	Primer	Sequence (5’ - 3’)
ALP	Forward	TGGTCACAGCAGTTGGTAGC
	Reverse	CTGAGATTCGTCCCTCGCTG
BMP2	Forward	CGGCGTCTCCTTTAAAAGCC
	Reverse	CTGGAGTTCCAACCCGTGTC
OPN	Forward	CCTGGCTGAATTCTGAGGGAC
	Reverse	CTTCTGAGATGGGTCAGGCA
COL-1	Forward	CCATCGGTCATGCTCTCTCC
	Reverse	CCATCGGTCATGCTCTCTCC
RUN×2	Forward	AGCTTTAGCGTCGTCAGACC
	Reverse	TTTCAAGGTGCCGGGAGGTA

2.9. Immunocytochemistry. Three types of media were prepared: disperse 5 mg cluster-loaded hydrogel into 50 mL α-MEM medium to obtain 100 μg/mL of cluster-loaded hydrogel dispersion (cluster-loaded hydrogel group); suspend 5 mg HAP particles in 50 mL α-MEM medium to obtain 100 μg/mL of HAP suspension (HAP group); or α-MEM medium only (control group). MC3T3-E1 cells cultured with control, HAP, and cluster-loaded hydrogel groups for 14 days were fixed with 4% paraformaldehyde (Solarbio, Beijing) and treated with 0.5% Triton X-100 (Solarbio, Beijing) for permeabilization. The MC3T3-E1 cells were incubated with 5% BSA (BBI, Shanghai) for blocking nonspecific binding of the primary antibodies and then incubated with antibodies against mouse monoclonal type-I collagen (COL-1), osteopontin (OPN), and runt-related transcription factor (RUN×2) at 4 ^{o}C overnight. The cells were then treated with fluorescent dye-conjugated secondary antibodies and incubated for 45 min at room temperature. All antibodies were purchased from Abcam. The fluorescent signals were observed under a fluorescence microscope.

2.10. Ex vivo bone affinity. The ex vivo rat bones without cells or vessels were kindly provided by the Animal Experiment Center of Zhejiang Chinese Medical University and the use of animal tissue for ex vivo study was approved by the guidelines and use of animals for scientific purposes issued by Zhejiang University. Three holes were drilled in the same bone and the diameter of each was approximately 2 mm. Each hole was not pierced through the bottom of the rat bone. The cluster-loaded hydrogel was synthesized by the above method and suspension of HAP particles was made by suspending the commercial HAP particles in PBS. In the experiment, the cluster-loaded hydrogel and suspension of HAP particles were injected into the holes marked by #3, and #2, respectively (Figure 8A), and the last empty hole marked by #1 was used as the control group. The HAP suspension and cluster-loaded hydrogel are thick fluids so they were retained in the defective area. The bone was then incubated in a water bath at 37 ^{o}C for 7 days. After that, the bone was dried at room temperature and kept for further experiments; the entire process of the bone affinity experiments was not maintained under sterile conditions.

2.11. In vivo bone regeneration. All animal experiments were performed at the Animal Research Center of Zhejiang Chinese Medical University. The handling of animals was carried out according to the guidelines and use of animals for scientific purposes issued by the Zhejiang University and Zhejiang Chinese Medical University. Thirty 8-week-old female Sprague-Dawley rats (body weight 290–330 g) were randomly divided into five groups: a control group (without any materials used); a PAA/PASP group (the PAA/PASP hydrogel was injected into the calvarial defects); an HAP group (a suspension of commercial HAP nanoparticles was placed into the calvarial defects); a cluster-loaded hydrogel group (the cluster-loaded hydrogel was injected into the calvarial defects); and a collagen-based bionic bone-matrix (Tian Sannie Bioengineering Technology Co., Ltd.) group (n = 6). In these experiments, the collagen-based bionic bone-matrix

consisted of HAP and collagen fibrils, which is currently used for bone substitution for clinically cured patients who suffer from bone defects. The collagen-based bionic bone-matrix is radio-opaque and is a biosafety composite material that, enables the growth of bone cells in the collagen-based bionic bone-matrix to form a bone-substitution material.[33] Subsequently, the in vivo bone regeneration performance of the cluster-loaded hydrogel was evaluated by using a widely used rat calvarial defect model.[34] Calvarial defects were generated using a trephine drill with a diameter of 5 mm on the bilateral sides of the midline in each rat calvarial, which cannot heal naturally during the lifetime of the rat because the rat calvarial lacks a blood supply and muscle tissue.[9] During the drilling process, 0.9% saline solutions were used for irrigation. All the materials were sterilized by ultraviolet radiation for 24 h. Both defects were treated with no treatment (control group), cluster-loaded hydrogel, PAA/PASP hydrogel, suspension of HAP particles, or collagen-based bionic bone-matrix, respectively. The latter has been clinically used for clinical human bone regeneration and was used here as a positive control (P-control). Then, the wounds were carefully sutured and the rats received penicillin on the first post-surgery day. All rats were sacrificed two or ten weeks later and their cranium specimens were harvested and used for histological observations.

2.12. Micro-CT scanning. Two or ten weeks after the calvarial defect operation, the rats were sacrificed, and the defect sites were removed intact with the surrounding bone prior to fixation in 10% neutral formaldehyde solution for 4 days. Each specimen was subjected to microcomputed tomography scanning using a desktop micro-CT scanner's auxiliary software that was set at a voltage of 80 kV and a current of 80 μA. The micro-CT scanner's auxiliary software was used to construct a 3D reconstruction from sequential scans. The bone volume fraction (BVF) and bone mineral density (BMD) in the defects were measured by the CTAn program.

2.13. Mechanical performance analysis. In the ex vivo bone affinity experiments, the Young's moduli and hardness of the HAP regenerated bone and cluster-loaded hydrogel regenerated bone was compared to the surrounding natural calvarial bone. The regenerated bones and surrounding bones were obtained by cutting the rat bone into 2 mm-high cylinders. In the in vivo bone regeneration experiments, the regeneration bones and natural bones were cut into small slices to measure their Young's moduli and hardness. A nanoindentation test was used for analysing the moduli and hardness of all the samples (G200, Agilent Technologies, CA, USA). Testworks 4 software was used to record and manage the experimental data (MTS System Corporation, Eden Prairie, MN, USA).

2.14. Statistical analysis. Triplicate experiments were performed. The results were expressed as the arithmetic ± standard deviation. Their statistical significance was tested by analysis of variance, followed by one-way ANOVA, and the p value lower than 0.05 was considered to indicate statistical significance.

3. RESULTS AND DISCUSSION

3.1. The formation and application of the cluster-loaded hydrogel. During synthesis, PAA and PASP are both negatively charged due to their carboxylate groups, so they can chelate with Ca^{2+} and form a hydrogel when their molecular weight is relatively high. To form the hydrogel phase, high molecular weight (450 kDa) PAA was used, which however rapidly precipitates when mixed with a high concentration of Ca^{2+}. Therefore, a lower molecular weight (9–11 kDa) PASP was first mixed with Ca^{2+} in our reaction in order to prevent precipitation. In this experiment, we were trying to maximize the Ca^{2+} in the hydrogel at 43.5 mM so that it can effectively repair bone defects. The cluster-loaded hydrogel has amorphous calcium phosphate (ACP) nanoclusters

loaded within the PAA/PASP hydrogel. Due to the small size effect of the ACP nanoclusters, the cluster-loaded hydrogel is liquid-like so that it can be directly injected into rat calvarial defects for regeneration (Figure 1).

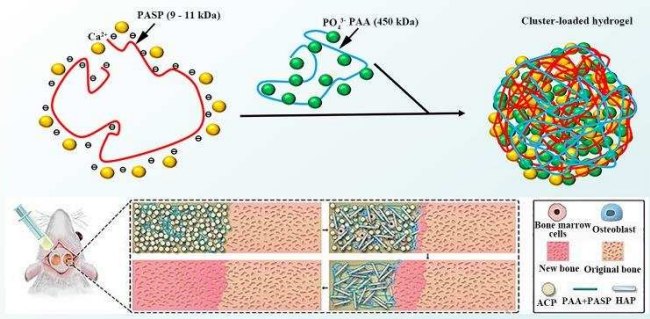

Figure 1. Preparation of the cluster-loaded hydrogel and its application in rat calvarial bone defective regeneration.

3.2. Morphology and properties of the hydrogel. The hydrogel loaded with ACP clusters is nearly transparent and free-flowing (Figure 2A). Close-to-focus cryogenic transmission electron microscopy (cryoTEM) images showed the size of the clusters are nearly 1 nm (Figure 2B). Selected area electron diffraction (SAED) revealed that the clusters are amorphous (inset of Figure 2B). The cluster size distribution in the hydrogel was measured by dynamic light scattering (DLS). As shown in Figure 2C, the dominant particle size of the clusters is ~1.4 nm. The features of the cluster-loaded hydrogel are related to its rheological properties. As shown in Figure 2D, the dynamic storage modulus (G') is very close to the loss modulus (G''), indicating the liquid state of the hydrogel with a slightly dominant role of viscosity. Over time, the G' and G'' increase at almost the same rate until a balance point was reached after 200 s of incubation, indicating the well formation of the cluster-loaded hydrogel (Figure 2E). The X-ray diffraction (XRD) data of the commercial amorphous calcium phosphate (ACP) and cluster-loaded hydrogel both showed a broad peak at approximately $2\theta = 30°$ (Figure 2F), indicating the clusters in the hydrogel are ACP.

The structure of the clusters was examined by Fourier transform infrared (FT-IR) spectrum, which shows two wide bands at 1055 and 560 cm^{-1} that can be attributed to the phosphate stretching (v_3) and phosphate bending (v_4) modes of the amorphous phase, respectively (Figure 2G).[35] The X-ray photoelectron spectra (XPS) depth profile further confirmed that the clusters contain both calcium and phosphorus elements (Figure 2H and 2I). These results indicate that the clusters loaded in the hydrogel are ACP.

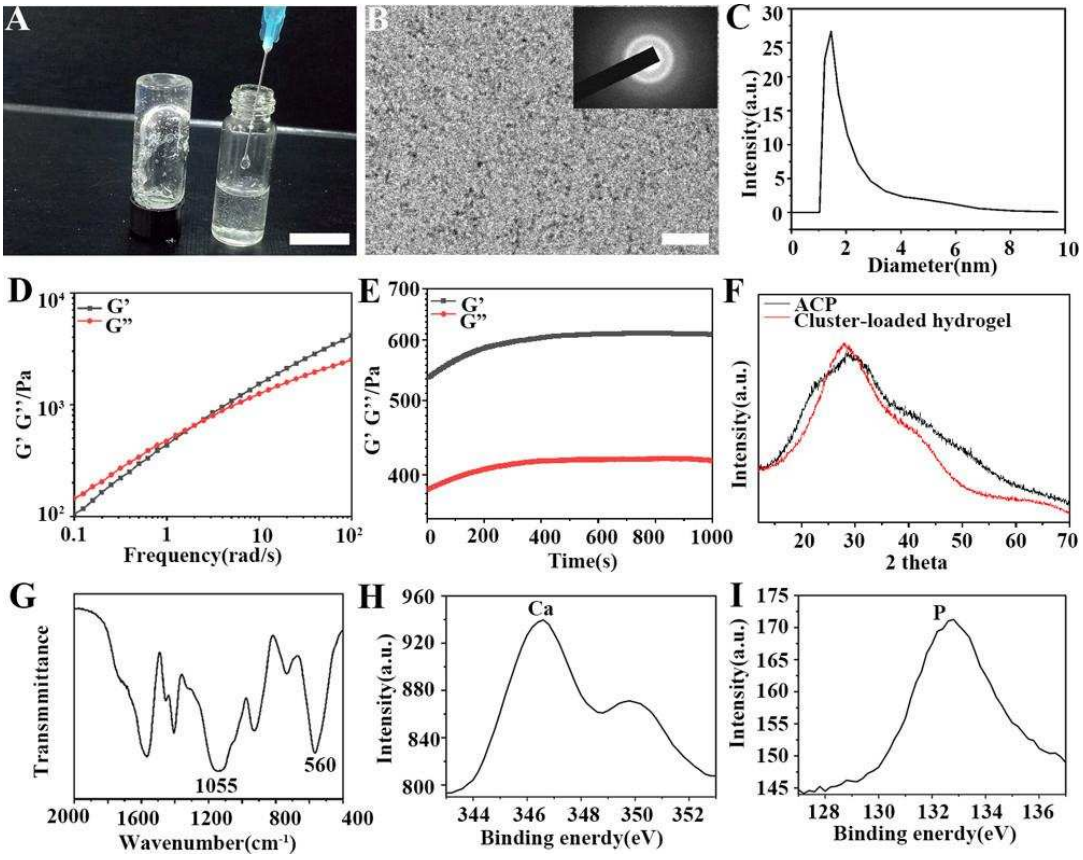

Figure 2. (A) Photo of the hydrogel, indicating the material has good fluidity. (B) Close-to-focus cryoTEM image of the cluster-loaded hydrogel, showing the size of the nanocluster is approximately 1 nm. The SAED showed that the clusters in hydrogel are amorphous. (C) DLS size distribution of the nanoclusters. (D) Rheological behavior of the cluster-loaded hydrogel. Frequency dependencies of the storage (G') and loss (G'') moduli. (E) Fitting curves of the cluster-

loaded hydrogel G' and G'' measured over time at a frequency = 1 rad s^{-1}. (F) The pXRD spectrum of the obtained hydrogel and commercial ACP. (G) The FT-IR spectrum of the hydrogel. (H) The XPS C 1s peaks of calcium atom in the hydrogel. (I) The XPS C 1s peaks of phosphorus atom in the hydrogel. Scale bars: 1 cm (A), 10 nm (B).

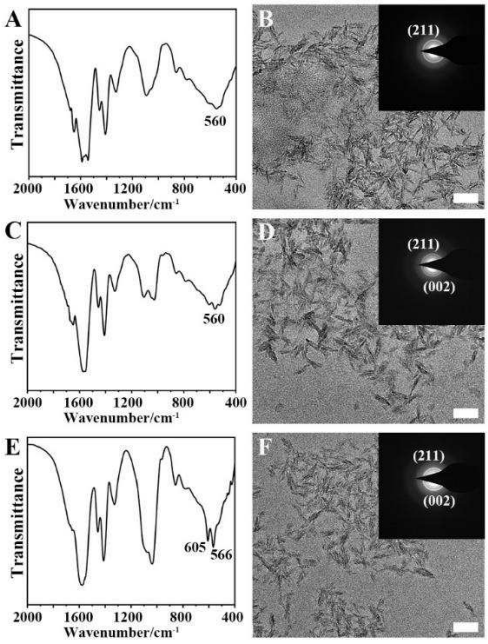

Figure 3. FT-IR spectrum of the cluster-loaded hydrogel at 37 ºC for 1 day (A), 3 days (C), 7 days (E), and TEM image and SAED image (inset) of the cluster-loaded hydrogel at 37 ºC for 1 day (B), 3 days (D), 7 days (F). Scale bars: 50 nm.

The cluster-loaded hydrogel transformed into HAP after being heated at 37 ºC for 7 days as shown by the FT-IR spectra, which over time showed the appearance of the HAP phosphate v_4 bending vibrations at 566 and 605 cm^{-1}, while the broad band at 560 cm^{-1} gradually disappears (Figure 3A, 3C and 3E). The selected area electron diffraction (SAED) analysis further demonstrated the transformation process, showing the increase in the reflections corresponding to the (002) and (211) planes of HAP over time (insets in Figure 3B, 3D, and 3F). TEM showed that the clusters

transformed into nanorod-like structures with a width/breadth of the HAP of approximately 50 × 4 nm, and the size barely changed for the crystallization process (Figure 3B, 3D, and 3F). In these experiments, ACP is the amorphous precursor phase, while HAP is the relatively stable state of calcium phosphate. The solidification and crystallization of the cluster-loaded hydrogel is related to the conversion of the ~1 nm clusters, which is similar to the 0.7–1.0 nm sized "Posner's clusters".[36,37] These clusters can form larger ACP particles, and then spontaneously assemble and solidify into crystalline HAP.[38]

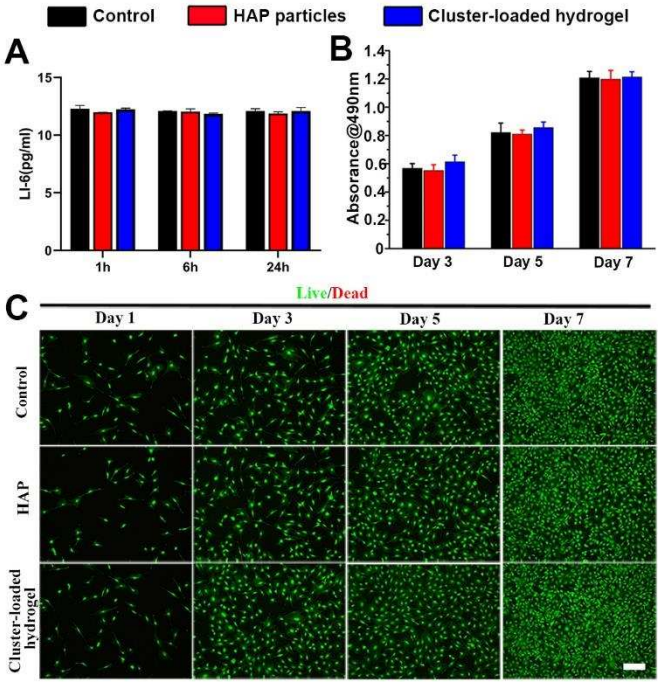

Figure 4. (A) The expression of IL-6 in the three groups. (B) Cell proliferation of the MC3T3-E1 cells after incubation for 3, 5, and 7 days. (C) The live/dead staining of MC3T3-E1 cells after incubation for 1, 3, 5, and 7 days. Scale bar: 200 nm.

3.3. Ex vivo biocompatibility. The IL-6 secretion by the RAW264.7 cells was tested to detect the inflammatory response of the HAP suspension and cluster-loaded hydrogel dispersion. The cluster-loaded hydrogel group showed a similar IL-6 release compared to the HAP and control

groups after culturing for 1, 6, and 24 h, indicating that there is no excessive secretion of IL-6 in the cluster-loaded hydrogel and HAP groups (Figure 4A). To test the biocompatibility of the cluster-loaded hydrogel, the viability and proliferation of the MC3T3-E1 cells were tested by live/dead staining and CCK-8. It is noteworthy that the number of live cells on the cluster-loaded hydrogel was similar to that on the HAP and control groups, revealing that the cluster-loaded hydrogel has good biocompatibility (Figure 4B and 4C).

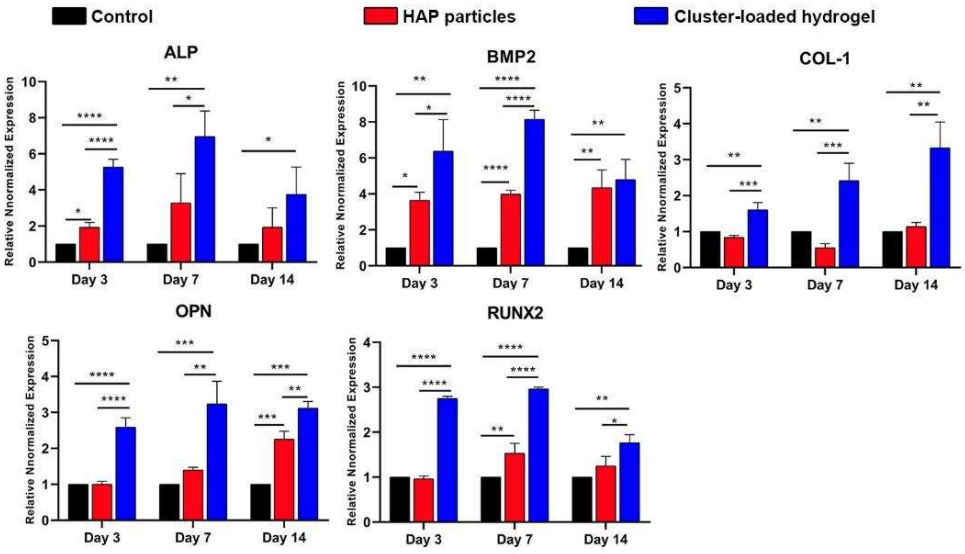

Figure 5. qPCR analysis to quantify the osteogenic marker gene expression in MC3T3-E1 cells grown for 3, 7, and 14 days with the control, HAP suspension, and cluster-loaded hydrogel dispersion groups, respectively. The mRNA expression of ALP, BMP2, COL-1, OPN and RUN×2 in the cluster-loaded hydrogel was significantly increased. n = 3, *p<0.05, ***p < 0.001.

3.4. Analysis of osteogenic induction. To confirm the bone regeneration purposes, we evaluated the osteoconductive capacity of the cluster-loaded hydrogel to promote the differentiation of MC3T3-E1 cells into an osteogenic lineage. The mRNA expression level in MC3T3-E1 cells was quantified by qPCR after culturing the cells for 3, 7, and 14 days under osteogenic medium

conditions. The osteogenic markers, including alkaline phosphate (ALP), bone morphogenetic protein-2 (BMP2), collagen type I (COL-1), osteopontin (OPN), and runt-related transcription factor 2 (RUN×2), were measured.[39] we found the MC3T3-E1 cells cultured with the cluster-loaded hydrogel expressed higher levels of all osteogenic markers than those cultured on HAP and in the control groups (Figure 5).

In addition, to confirm their potent expression in the MC3T3-E1 cells, immunofluorescence staining for OPN, COL-1, and RUN×2 was conducted after incubating the cells with different media for 14 days. As showed in figure 6, the MC3T3-E1 cells cultured with the cluster-loaded hydrogel exhibited a higher level of OPN, COL-1 and RUN×2 expression than in the other two groups. In general, the cluster-loaded hydrogel provides a suitable physicochemical and biological microenvironment for the proliferation and differentiation of MC3T3-E1 cells, which is essential for in vivo tissue regeneration.

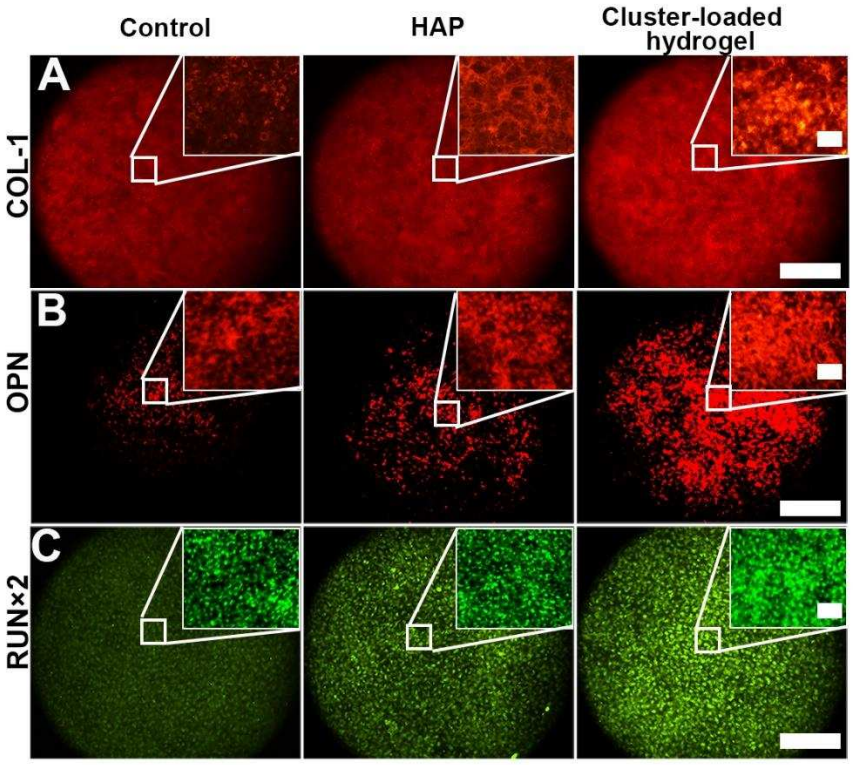

Figure 6. Immunofluorescence staining of COL, OPN, and RUN×2 in MC3T3-E1 cells after 14 days of culturing with the control, HAP suspension, and cluster-loaded hydrogel dispersion groups, respectively. Scale bar: 2000 μm (A – C), 100 μm (insets in A – C).

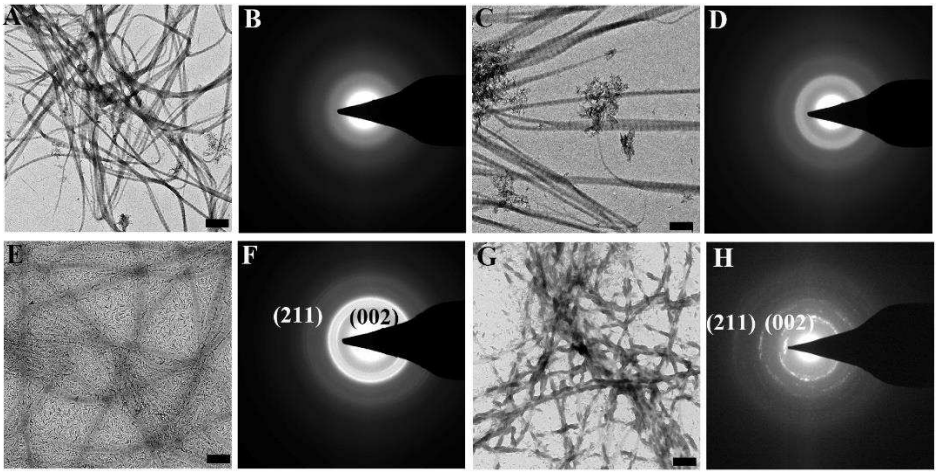

Figure 7. TEM images and SAED patterns of the native type-I collagen fibrils (A, B), and mineralized collagen fibrils by using commercial ACP particles (C, D), commercial HAP particles (E, F), and cluster-loaded hydrogel (G, H) at 37 ºC for 7 days. Scale bars: 500 nm.

3.5. Collagen mineralization. In bone formation, collagen fibrils are generally considered to be a scaffold and template for mineralization at the molecular level. Small amorphous ACP nanoclusters can penetrate into the collagen fibrils and form nucleation sites, which will convert into oriented HAP crystals inside the collagen, inducing intrafibrillar mineralization of the collagen fibrils.[18] The cluster-loaded hydrogel was also used for mineralizing collagen fibrils. The native type-I collagen fibrils display periodic overlap and gap zones (Figure 7A and 7B). After 7 days of contact with commercial ACP or HAP nanoparticles, the collagen fibrils hardly mineralized, the ACP nanoparticles assembled together (Figure 7C and 7D), and the HAP nanocrystals were in their original state (Figure 7E and 7F). TEM grids with attached collagen fibrils were floated over

the cluster-loaded hydrogel at 37 ºC for 7 days. The results showed that mineralization preferably occurs on/in the collagen fibrils, generating HAP with their c-axes on average aligned with the fibril axes, in line with previous reports (Figure 7G and 7H).[40]

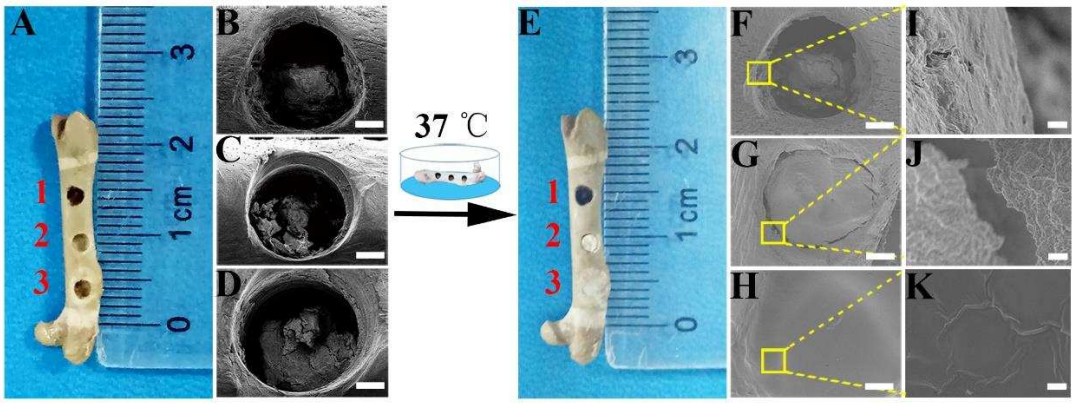

Figure 8. Ex vivo bone regeneration process. (A) Photo of the rat bone with three holes drilled for further experiment, which were marked by #1, 2 and 3. (B - D) SEM images of the holes #1, 2 and 3. (E) The photo of rat bone kept at 37 ºC for 7 days, with cluster-loaded hydrogel filled into #3 hole, suspension of HAP particles filled into #2 hole, and #1 hole remained empty as a control group. (F - H) SEM images of the #1, 2 and 3 hole after regeneration, with zoom-in images shown in (I - K), respectively. Scale bars: B – D and F – H are 500 μm, I – K is 20 μm.

3.6. Ex vivo bone affinity. For ex vivo bone regeneration experiments, three holes were drilled in the same rat bone, marked by #1, #2, and #3 (Figure 8A - D). The hole marked by #3 was injected with the cluster-loaded hydrogel, while the hole marked by #2 was injected with the suspension of HAP particles, and the empty hole #1 was used as the control group (Figure 8E). After incubation in a 37 ºC water bath for 7 days, scanning electron microscopy (SEM) showed that a continuous filling was formed within hole #3 (Figure 8H and K), while very poor filling was observed in hole #1 (Figure 8F and I) and in hole #2 gaps were observed between the filling and the rat bone (Figure

8G and J). The results showed that the cluster-loaded hydrogel has a good affinity to natural rat bone. The mechanical properties of the repaired bone and natural bone were also tested. The results showed that the Young's moduli and the hardness value of the HAP recovered bone, cluster-loaded hydrogel treated bone and natural bone were 3.7 GPa and 79.8 MPa, 13.4 GPa and 300.4 MPa, 13.9 GPa and 300.8 MPa, respectively (Figure 9A and 9B), indicating the mechanical performances of the hydrogel treated bone are comparable with natural bone.

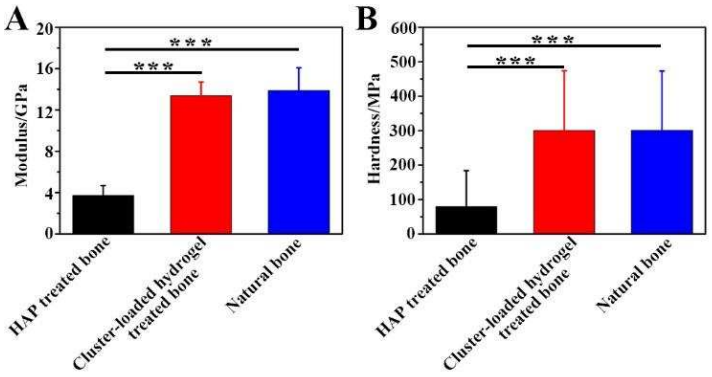

Figure 9. Young's modulus (A) and hardness (B) of the three groups, n = 6, ***p < 0.001.

3.7. In vivo bone regeneration. All the rats remained in good health and did not show any wound symptoms throughout the two or ten weeks of experiments. After injection, the hydrogel was observed to completely fill up the bone defect area (Figure 10).

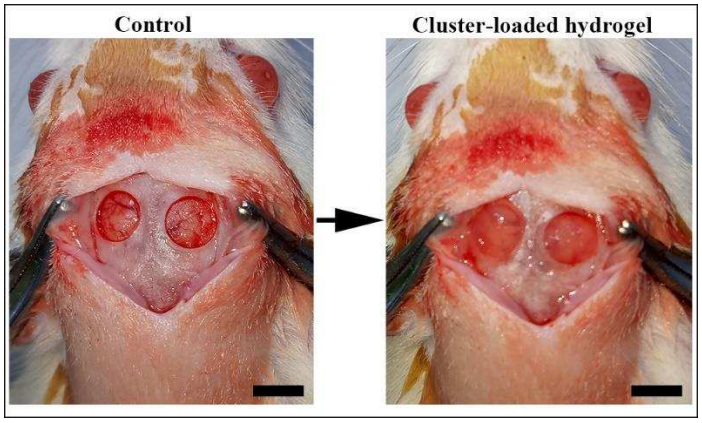

Figure 10. Schematic of the surgical operation that placed the cluster-loaded hydrogel to seal off the calvarial defects of rats. Scale bar: 5 mm.

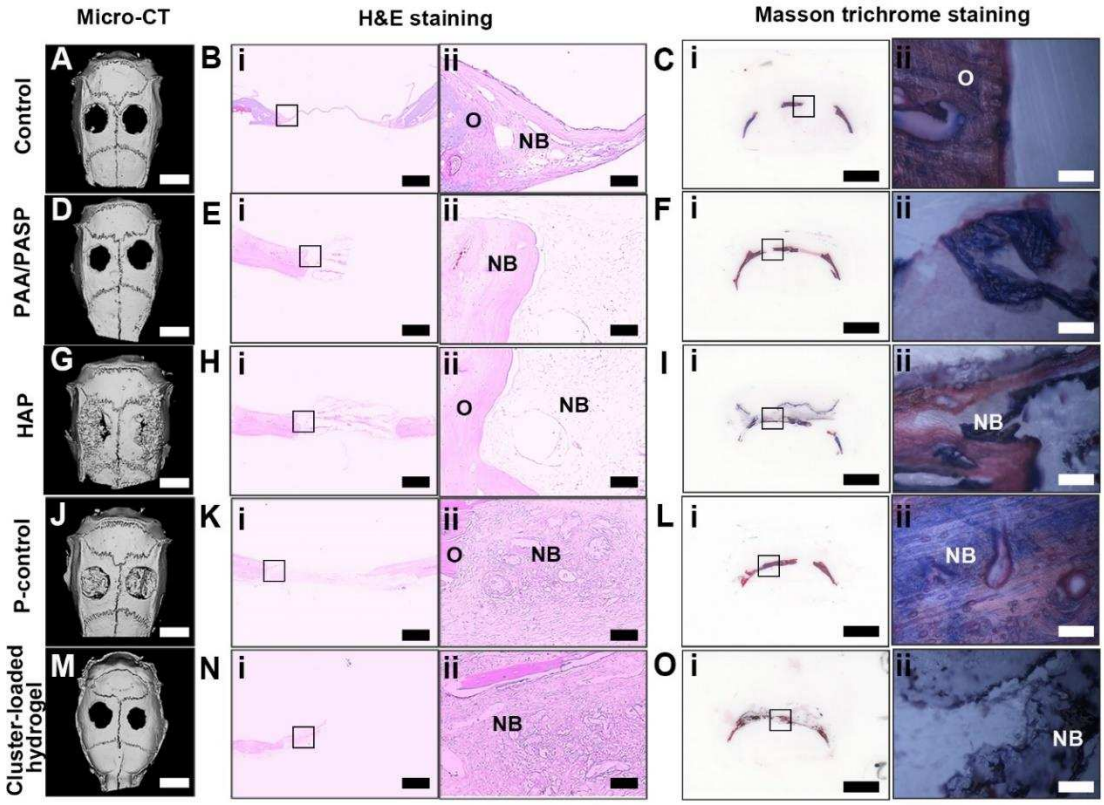

Figure 11. *In vivo* bone regeneration of control, PAA/PASP, HAP, P-control and cluster-loaded hydrogel groups after two weeks. (A, D, G, J, M) Representative reconstructed micro-CT images. (B, E, H, K, N) Representative H&E staining results, with zoom-in images of the bone defect margins (black rectangles). (C, F, I, L, O) Representative Masson trichrome staining results, with zoom-in images of the bone defect margins (black rectangles). NB: new bone; O: Original bone. Scale bars: 5 mm (A, D, G, J, M), 1 mm (B(i), E(i), H(i), K(i), N(i)), 50 μm (B(ii), E(ii), H(ii), K(ii), N(ii)), 2 mm (C(i), F(i), I(i), L(i), O(i)), 100 μm (C(ii), F(ii), I(ii), L(ii), O(ii)).

Micro-CT, haematoxylin and eosin (H&E) staining and Masson trichrome staining were performed two weeks and ten weeks after treatment, in order to study the quantity of the

regenerated bone. After two weeks, reconstructed micro-CT and H&E staining images showed no significant new bone formation in the calvarial defects collected from the control and PAA/PASP groups (Figures 11A - B and D - E). The HAP group showed a high amount of minerals (Figure 11G); however, the amount of new bone was relatively low, indicating the HAP maintained its original state and that there was only a small amount of new bone formation induced in the HAP group (Figure 11H). Although the P-control group showed significant new bone formation (Figure 11J - K), a gap could be observed between the surrounding bone and the filling material. Meanwhile, a small amount of bone regeneration was observed along the margin of the calvarial bone in the cluster-loaded hydrogel group (Figure 11M - N), indicating the cluster-loaded hydrogel indeed facilitated a small amount of new bone formation at two weeks. To examine the maturity of the newly formed bone, Masson trichrome staining was performed. As shown in Figure 11C, F, I, L, and O, blue mature bone was detected in the calvarial in the P-control and cluster-loaded hydrogel groups, suggesting the newly formed bone had undergone maturation.

After ten weeks, the reconstructed micro-CT, H&E staining, and Masson trichrome staining images of the control and PAA/PASP groups showed a low amount of bone formation along the margins of the defective area with hardly any new bone formation at the center of the defect (Figure 12A - B and D - E). The amount of HAP particles at ten weeks was decreased in comparison with that at two weeks, indicating the degradation of the HAP (Figure 12G - H). The state of the bone regeneration in the P-control group after ten weeks was similar to that after two weeks, and a gap between the native bone and filling material could also be observed (Figure 12J - K). In contrast, the group treated with the cluster-loaded hydrogel not only showed new bone formation comparable with the P-control group, but also had newly formed bone continuously distributed over the entire fracture. Additionally, the new bone contained a higher number of small vascular

channels, which can probably facilitate the differentiation of new bone from the native bone, and enable efficient cell growth in the defective area (Figure 12M - N). The Masson trichrome staining in vivo at ten weeks in the five groups provided the supplementary information for H&E staining (Figure 12C, F, I, L, and O). At ten weeks, hardly any new bone was found in the control, PAA/PASP and HAP groups (Figure 12C, F and I); however, a large amount of new bone tissue and mature bone were found and the materials almost disappeared for the cluster-loaded hydrogel group (Figure 12O). Meanwhile, some new bone tissues were also found for the P-control group, but there was low amount of residual materials (Figure 12L). The amount of new vasculature was also estimated, which was approximately 3% in the cluster-loaded hydrogel group. This value is similar to the the regeneration performance of the integrin-specific hydrogels.[41]

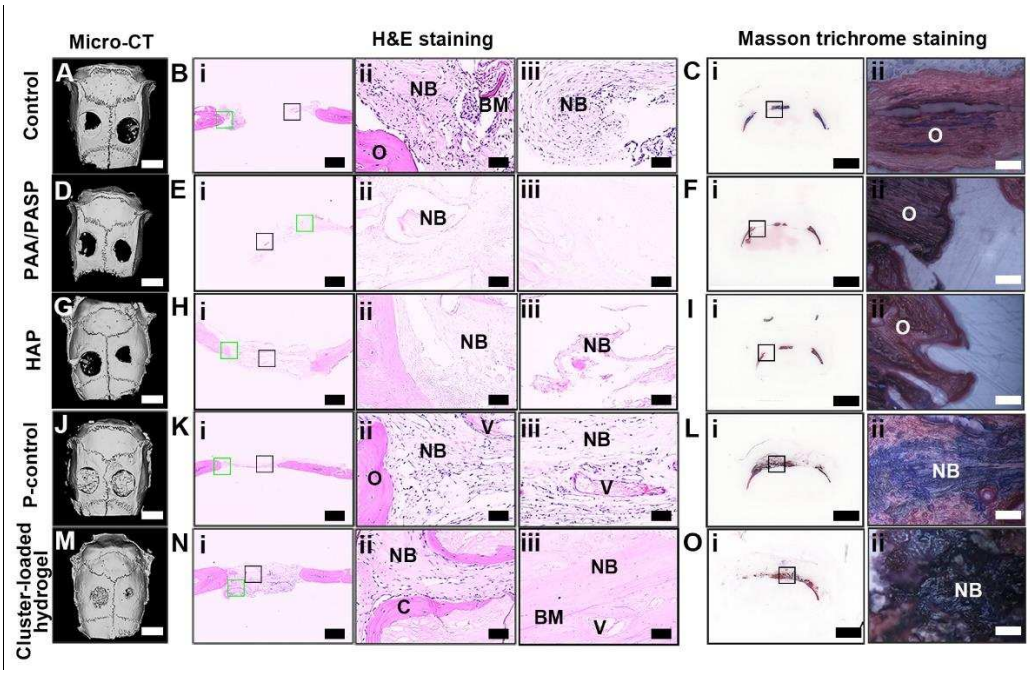

Figure 12. *In vivo* bone regeneration of control, PAA/PASP, HAP, P-control and cluster-loaded hydrogel group after ten weeks. (A, D, G, J, M) Representative reconstructed micro-CT images. (B, E, H, K, N) Representative H&E staining results, with zoom-in images of the bone defect

margins (green rectangles) and defect center (black rectangles). (C, F, I, L, O) Representative Masson trichrome staining results, with zoom-in images of the bone defect regions (black rectangles). NB: new bone; O: Original bone; BM: bone marrow cells; V: vessel; C: cluster-loaded hydrogel. Scale bars: 5 mm (A, D, G, J, M), 1 mm (B(i), E(i), H(i), K(i), N(i)), 50 μm (B(ii-iii), E(ii-iii), H(ii-iii), K(ii-iii), N(ii-iii)), 2 mm (C(i), F(i), I(i), L(i), O(i)), 100 μm (C(ii), F(ii), I(ii), L(ii), O(ii)).

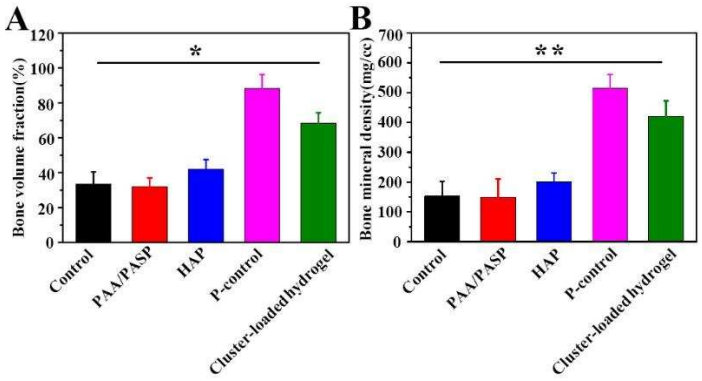

Figure 13. (A) Micromorphometric bone parameters BVF analysed after 10 weeks of surgery. (B) Micromorphometric bone parameters BMD analysed after 10 weeks of surgery. In (A) and (B), n = 6, $^{*}p < 0.05$.

The bone volume fraction (BVF) of the hydrogel group was 68%, while the control group was approximately 33% (Figure 13A). As a major index for the evaluation of the quality and strength of the regenerated bone, bone mineral density (BMD) was also analysed. The BMD of the hydrogel group was approximately 3 times higher than the control group (Figure 13B). These results demonstrated that the cluster-loaded hydrogel can effectively enhance the bone cells bioactivity and promote bone healing in bone defects.

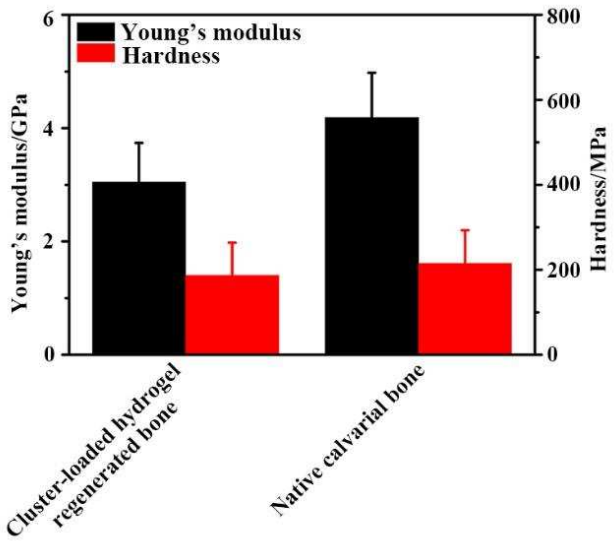

Figure 14. Young's modulus and hardness of the cluster-loaded hydrogel regenerated bone and surrounding native calvarial bone.

To explore the mechanical properties of the regenerated calvarial bone, we used nanoindentation to measure the Young's modulus and hardness of the cluster-loaded hydrogel regenerated bone and its surrounding native calvarial bone. The values for Young's modulus of the cluster-loaded hydrogel regenerated bone and the surrounding bone were found to be in the same range (3.05 and 4.19 GPa, respectively). The hardness of the cluster-loaded hydrogel regenerated bone and surrounding native calvarial bone were 187 and 215 MPa, respectively (Figure 14). These data indicate that the cluster-loaded hydrogel regenerated bone has a mechanical performance matching the surrounding native rat bone.

4. CONCLUSIONS

In this work, we developed an ACP cluster-loaded hydrogel for bone regeneration as an alternative to traditional bone-regeneration materials. This free-flowing hydrogel can efficiently fill rat bone defects, regenerating bone tissues that are tightly bound to the native tissue. The newly formed

bones show mechanical performance comparable with the native bone, and no adverse effect was observed during the treatment. The ability of this injectable hydrogel to fill bone defects of varying geometries allows clinical bone defect treatment without a surgical incision. We attribute the unique properties of this hydrogel to its microstructure, which resembles the biological matrix in vivo and contains ACP clusters that can facilitate intrafibrillar HAP formation. Our work provides a good example of how in-depth understanding of biomineralization processes can lead to new developments in regenerative medicine.

AUTHOR INFORMATION

Corresponding Author

* E-mail: rtang@zju.edu.cn Fax: (+) 86-571-87953736

Notes

The authors declare no competing financial interest.

■ ACKNOWLEDGEMENTS

This research was supported by the Nation Key R&D program of China (2018YFC1105101), the National Natural Science Foundation of China (21625105, and 21571155) and the Fundamental Research Funds for the Central Universities. The research of Y.X. was supported by a TOP-PUNT grant from the Netherlands Organization of Scientific Research.

■ REFERENCES

(1) Weiner, S.; Wagner, H. D. The Material Bone: Structure-Mechanical Function Relations. Annu. Rev. Mater. Sci. **1998,** 28(1), 271-298.

(2) Palmer, L. C.; Newcomb, C. J.; Kaltz, S. R.; Spoerke, E. D.; Stupp, S. I. Biomimetic Systems for Hydroxyapatite Mineralization Inspired by Bone and Enamel. Chem. Rev. **2008,** 108(11), 4754-4783.
(3) Raajimakers, M. H.; Mukherjee, S.; Guo, S.; Zhang, S.; Kobayashi, T.; Schoonmaker, J. A.; Scadden, D. T. Bone Progenitor Dysfunction Induces Myelodysplasia and Secondary Leukaemia, Nature, **2010**, 464(7290), 852-857.
(4) Murugan, R.; Ramakrishna, S. Development of Nanocomposites for Bone Grafting. Compos. Sci. Technol. **2005,** 65(15), 2385-2406.
(5) Alvarez, K.; Nakajima, H. Metallic Scaffolds for Bone Regeneration. Materials **2009,** 2(3), 790-832.
(6) Uchida, A.; Araki, N.; Shinto, Y.; Yoshikawa, H.; Kurisaki, E.; Ono, K. The Use of Calcium Hydroxyapatite Ceramic in Bone Tumour Surgery. Bone Joint J. **1990,** 72(2), 298-302.
(7) Wang, M. O.; Vorwald, C. E.; Dreher, M. L.; Mott, E. J.; Cheng, M. H.; Cinar, A.; Mehdizadeh, H.; Somo, S.; Dean, D.; Brey, E. M. *Evaluating 3D-Printed* Biomaterials as Scaffolds for Vascularized Bone Tissue Engineering. Adv. Mater. **2015,** 27(1), 138-144.
(8) Liu, Y.; Liu, S.; Luo, D.; Xue, Z.; Yang, X.; Gu, L.; Zhou, Y.; Wang, T. Hierarchically *Staggered Nanostructure of Mineralized Collagen as a Bone-Grafting Scaffold*. Adv. Mater. **2016,** 28(39), 8740-8748.
(9) Lu, J.; Cheng, C.; He, Y. S.; Lyu, C.; Wang, Y.; Yu, J.; Qiu, L.; Zou, D.; Li, D. Multilayered Graphene Hydrogel Membranes for Guided Bone Regeneration. Adv. Mater. **2016,** 28(21), 4025-4031.
(10) Nonoyama, T.; Wada, S.; Kiyama, R.; Kitamura, N.; Mredha, M.; Islam, T.; Zhang, X.; Kurokawa, T.; Nakajima, T.; Takagi, Y. *Double-Network Hydrogels Strongly Bondable to Bones* by Spontaneous Osteogenesis Penetration. Adv. Mater. **2016,** 28(31), 6740-6745.
(11) Laurenti, M.; Al Subaie, A.; Abdallah, M. N.; Cortes, A. R.; Ackerman, J. L.; Vali, H.; Basu, K.; Zhang, Y. L.; Murshed, M.; Strandman, S. Two-Dimensional Magnesium Phosphate Nanosheets Form Highly Thixotropic Gels That Up-Regulate Bone Formation. Nano Lett. **2016,** 16(8), 4779-4787.
(12) Levi-Kalisman, Y.; Falini, G.; Addadi, L.; Weiner, S. Structure of the Nacreous Organic Matrix of a Bivalve Mollusk Shell Examined in the Hydrated State Using Cryo-TEM. J. Struct. Biol. **2001,** 135(1), 8-17.
(13) Murayama, E.; Takagi, Y.; Ohira, T.; Davis, J. G.; Greene, M. I.; Nagasawa, H. Fish Otolith Contains a Unique Structural Protein, O*tolin-1*. Eur. J. Biochem. **2002,** 269(2), 688-696.
(14) Moradian-Oldak, J. Amelogenins: Assembly, Processing and Control of Crystal Morphology. Matrix Biol. **2001,** 20(5), 293-305.
(15) Weiner, S.; Traub, W.; Wagner, H. D. Lamellar Bone: Structure–Function Relations. J. Struct. Biol. **1999,** 126(3), 241-255.
(16) Clode, P. L.; Marshall, A. Calcium Associated with a Fibrillar Organic Matrix in the Scleractinian Coral Galaxea Fascicularis. Protoplasma **2003,** 220(3), 153-161.
(17) Estroff, L. A.; Addadi, L.; Weiner, S.; Hamilton, A. D. An Organic Hydrogel as a Matrix for the Growth of Calcite Crystals. Org. Biomol. Chem. **2004,** 2(1), 137-141.
(18) Madhumathi, K.; Shalumon, K. T.; Divya Rani, V. V.; Tamura, H.; Furuike, T.; Selvamurugan, N.; Nair, S. V.; Jayakumar, R. Wet Chemical Synthesis of Chitosan Hydrogel-Hydroxyapatite Composite Membranes for Tissue Engneering Application. Int. J. biol. Macromol. **2009**, 45(1), 12-15.

(19) Amosi, N.; Zarzhitsky, S.; Gilsohn, E.; Salnikov, O.; Monsonego-Ornan, E.; Shahar, R.; Rapaport, H. Acidic Peptide Hydrogel Scaffolds Enhance Calcium Phosphate Mineral Turnover into Bone Tissue. Acta Biomater. **2012**, 8(7), 2466-2475.
(20) Bendtsen, S. T.; Quinnell, S. P.; Wei, M. Development of a Novel Alginate-Polyvinyl Alcohol-Hydroxyapatite Hydrogel for 3D Bioprinting Bone Tissue Engineering Scaffolds. J. Biomed. Mater. Res. **2017**, 105(5), 1457-1468.
(21) Struillou, X.; Boutigny, H.; Badran, Z.; Fellah, B. H.; Gauthier, O.; Sourice, S.; Pilet, P.; Rouillon, T.; Layrolle, P.; Weiss, P.; Soueidan, A. Treatment of Periodontal Defects in Dogs Using an Injectable Composite Hydrogel/Biphasic Calcium Phosphate. J. Mater. Sci: Mater. Med. **2011**, 22(7), 1707-1717.
(22) Zhao, L.; Weir, M. D.; Xu, H. H. An Injectable Calcium Phosphate-Alginate Hydrogel-Umbilical Cord Mesenchymal Stem Cell Paste for Bone Tissue Engineering. Biomaterials **2010**, 31, 6502-6510.
(23) Nudelman, F.; Pieterse, K.; George, A.; Bomans, P. H. H.; Friedrich, H.; Brylka, L. J.; Hilbers, P. A. J.; de With, G.; Sommerdijk, N. The Role of Collagen in Bone Apatite Formation in the Presence of Hydroxyapatite Nucleation Inhibitors. Nat. Mater. **2010,** 9(12), 1004-1009.
(24) Dey, A.; Bomans, P. H.; Müller, F. A.; Will, J.; Frederik, P. M.; Sommerdijk, N. A. The Role of Prenucleation Clusters in Surface-Induced Calcium Phosphate Crystallization. Nat. Mater. **2010,** 9(12), 1010-1014.
(25) Habraken, W. J.; Tao, J.; Brylka, L. J.; Friedrich, H.; Bertinetti, L.; Schenk, A. S.; Verch, A.; Dmitrovic, V.; Bomans, P. H.; Frederik, P. M. Ion-Association Complexes Unite Classical and Non-Classical Theories for the Biomimetic Nucleation of Calcium Phosphate. Nat. Commun. **2013,** 4, 1507-1519.
(26) Niu, L. N.; Jee, S. E.; Jiao, K.; Tonggu, L.; Li, M.; Wang, L.; Yang, Y.-d.; Bian, J. H.; Breschi, L.; Jang, S. S. Collagen Intrafibrillar Mineralization as a Result of the Balance Between Osmotic Equilibrium and Electroneutrality. Nat. Mater. **2017,** 16(3), 370-378.
(27) Ye, J.; Wang, D.; Zeiger, D. N.; Miles, W. C.; Lin-Gibson, S. Different Kinetic Pathways of Early Stage Calcium-Phosphate Cluster Aggregation Induced by Carboxylate-Containing Polymers. Biomacromolecules **2013,** 14(10), 3417-3422.
(28) Krogstad, D. V.; Wang, D.; Lin-Gibson, S. Polyaspartic Acid Concentration Controls the Rate of Calcium Phosphate Nanorod Formation in High Concentration Systems. Biomacromolecules **2017,** 18(10), 3106-3113.
(29) Olszta, M. J.; Cheng, X.; Jee, S. S.; Kumar, R.; Kim, Y. Y.; Kaufman, M. J.; Douglas, E. P.; Gower, L. B. Bone Structure and Formation: a New Perspective. Mat. Sci. Eng. R **2007,** 58(3), 77-116.
(30) Niu, L. N.; Jiao, K.; Ryou, H.; Yiu, C. K.; Chen, J. H.; Breschi, L.; Arola, D. D.; Pashley, D. H.; Tay, F. R. Multiphase Intrafibrillar Mineralization of Collagen. Angew. Chem. In. Ed. **2013,** 52(22), 5762-5766.
(31) Addison, W. N.; Nelea, V.; Chicatun, F.; Chien, Y. C.; Tran-Khanh, N.; Buschmann, M. D.; Nazhat, S. N.; Kaartinen, M. T.; Vali, H.; Tecklenburg, M. M.; Franceschi, R. T.; Mckee, M. D. Extracellular Matrix Mineralization in Murine MC3T3-E1 Osteoblast Cultures: an Ultrastructural, Compositional and Comparative Analysis with Mouse Bone. Bone, **2015**, 71, 244-256.
(32) Obiweluozor, F. O.; Tiwari, A. P.; Lee, J. H.; Batgerel, T.; Kim, J. Y.; Lee, D.; Park, C. H.; Kim, C. S. Thromboresistant Semi-IPN Hydrogel Coating: Towards Improvement of the

Hemocompatibility/Biocompatibility of Metallic Stent Implants. Mater. Sci. Eng. C **2019**, 99, 1274-1288.
(33) Wang, Z.; Zhang, C.; Xie, L. Biosafety Evaluation of Collagen-Based Bone Repairing Material. J. Biomed. Eng. **2013**, 30(1), 105-109.
(34) Cowan, C. M.; Shi, Y. Y.; Aalami, O. O.; Chou, Y. F.; Mari, C.; Thomas, R.; Quarto, N.; Contag, C. H.; Wu, B.; Longaker, M. T. Adipose-Derived Adult Stromal Cells Heal Critical-Size Mouse Calvarial Defects. Nat. Biotechnol. **2004,** 22(5), 560-567.
(35) Chou, Y. F.; Chiou, W. A.; Xu, Y.; Dunn, J. C.; Wu, B. M. The Effect of pH on the Structural Evolution of Accelerated Biomimetic Apatite. Biomaterials **2004,** 25(22), 5323-5331.
(36) Posner, A. S.; Betts, F. Synthetic Amorphous Calcium Phosphate and its Relation to Bone Mineral Structure. Acc. Chem. Res. **1975**, 8(8), 273-281.
(37) Onuma, K.; Ito, A. Cluster Growth Model for Hydroxyapatite. Chem. Mater. **1998**, 10(11), 3346-3351.
(38) Habraken, W. J.; Tao, J.; Brylka, L. J.; Friedrich, H.; Bertinetti, L.; Schenk, A. S.; Verch, A.; Dmitrovic, V.; Bomans, P. H.; Frederik, P. M.; Laven, J.; Schoot, P.; Aichmayer, B.; De with, G.; DeYereo, J. J.; Sommerdijk, N. A. Ion-Association Complexes Unite Classical and Non-Classicial Theories for the Biomimetic Nucleation of Calcium Phosphate. Nat. Commun. **2013**, 4, 1507-1519.
(39) Krishnamurithy, G.; Murali, M. R.; Hamdi, M.; Abbas, A. A.; Raghavendran, H. B.; Kamarul, T. Proliferation and Osteogenic Differentiation of Mesenchymal Stromal Cells in a Novel Porous Hydroxyapatite Scaffold. Regen. Med. **2015**, 10(5), 579-590.
(40) Shao, C.; Zhao, R.; Jiang, S.; Yao, S.; Wu, Z.; Jin, B.; Yang, Y.; Pan, H.; Tang, R. Citrate Improves Collagen Mineralization via Interface Wetting: a Physicochemical Understanding of Biomineralization Control. Adv. Mater. **2018**, 30, 1704876.
(41) García, J. R.; Clark, A. Y.; García, A. J. Integrin-Specific Hydrogels Functionalized with VEGF for Vascularization and Bone Regeneration of Critical-Size Bone Defects. J. Biomed. Mater. Res. A **2016**, 104(4), 889-900.

The injectable ACP cluster-loaded hydrogel can efficiently fill in rat bone defects in vivo, regenerating bone tissues with mechanical performance comparable with native bone.

ToC graphic